REPORT DOCUMENTATION PAGE

Form Approved
OMB NO. 0704-0188

1. AGENCY USE ONLY (Leave Blank)	2. REPORT DATE	3. REPORT TYPE AND DATES COVERED
	May 2003	Final Report

4. TITLE AND SUBTITLE Ceramic Bar-on-Bar Impact Experiments	5. FUNDING NUMBERS Grant No. DAAD19-01-1-0791
6. AUTHOR(S) Dr. N.S. Brar	
7. PERFORMING ORGANIZATION NAME(S) AND ADDRESS(ES) University of Dayton Research Institute 300 College Park Dayton, Ohio 45469-0110	8. PERFORMING ORGANIZATION University of Dayton Research REPORT NUMBER UDRI-TR-2003-00089
9. SPONSORING / MONITORING AGENCY NAME(S) AND ADDRESS(ES) U. S. Army Research Office P.O. Box 12211 Research Triangle Park, NC 27709-2211	10. SPONSORING / MONITORING AGENCY REPORT NUMBER 43000.1-EG

11. SUPPLEMENTARY NOTES

The views, opinions and/or findings contained in this report are those of the author(s) and should not be construed as an official Department of the Army position, policy or decision, unless so designated by other documentation.

12 a. DISTRIBUTION / AVAILABILITY STATEMENT	12 b. DISTRIBUTION CODE
Approved for public release; distribution unlimited.	

13. ABSTRACT (Maximum 200 words) Ceramic bar-on-bar (uniaxial stress) experiments are performed to extend uniaxial strain deformation states imposed in flyer plate impact experiments. The major objective of these experiments is to generate a variety of multiaxial deformation states for characterizing the failure mechanisms in ceramics and other brittle materials.

14. SUBJECT TERMS split Hopkinson Bar	15. NUMBER OF PAGES 26
	16. PRICE CODE

17. SECURITY CLASSIFICATION OR REPORT	18. SECURITY CLASSIFICATION ON THIS PAGE	19. SECURITY CLASSIFICATION OF ABSTRACT	20. LIMITATION OF ABSTRACT
UNCLASSIFIED	UNCLASSIFIED	UNCLASSIFIED	UL

TABLE OF CONTENTS

LIST OF FIGURES

LIST OF TABLES

ABSTRACT

Ceramic bar-on-bar (uniaxial stress) experiments are performed to extend uniaxial strain deformation states imposed in flyer plate impact experiments. The major objective of these experiments is to generate a variety of multiaxial deformation states for characterizing the failure mechanisms in ceramics and other brittle materials. A number of investigators engaged in modeling the bar-on-bar experiments have varying degrees of success in capturing the observed fracture modes in bars and correctly simulating the measured in-situ axial stress or free surface velocity histories (section 1.1). The difficulties encountered are related to uncertainties in understanding the dominant failure mechanisms as a function of different stress states imposed in bar impacts. Free surface velocity of the far end of the AD998 target bar are measured using a VISAR in a series of bar-on-bar impact experiments at nominal impact speeds of 100 m/s, 220 m/s, and 300 m/s. Velocity histories at an impact velocity of 100 m/s shows that the impact is elastic. At higher impact velocities of 200 m/s and 300 m/s, the velocity history data suggests an inelastic impact. A high-speed (Imacon) camera was employed to examine the fracture and failure of impactor and target bars. High-speed photographs will provide comprehensive data on geometry of damage and failure patterns as a function of time to check the validity of a particular constitutive material model for AD998 alumina used in numerical simulations of fracture and failure of the bars on impact.

This work was performed under US Army Research Office (ARO) Grant No. DAAD19-01-1-0791. Dr. A.M. Rajendran of ARO was the technical contact and provided the general instructions concerning experimental configuration and other relevant information for the project. University of Dayton Research Institute Project supervision was provided by Mr. Michael P. Bouchard, Head, Aerospace Mechanics Division, and Mr. Kevin L. Poormon, Impact Physics Group Leader. Dr. N. S. Brar was the Principal Investigator with experimental assistance provided by Dr. W. Proud of the Cavendish Laboratory of the University of Cambridge, UK.

SECTION 1
BACKGROUND

1.1 Ceramic Bar-on-Bar Impact Experiments and Results

Bar impact has been widely used to study failure in brittle materials. Bar impact experiments are conducted by impacting a specimen bar, about 4-10 diameters long, either with a flyer plate or a bar impactor (bar-on-bar impact) of the same material or of a material of known Hugoniot. Strain rates produced in the bar target (~10^4/s) bridge the gap between the strain rates achieved in split Hopkinson bar (10^2-10^3/s) and flyer plate planar impact tests (10^5-10^7/s). Bar impacts on ductile materials provide data on flow or failure stress at a strain rate of ~10^4/s.[1-2] Various investigators[3-10] have conducted bar impact tests on brittle materials (e.g., rocks, concrete, glasses, ceramics), beginning with the pioneering research by Janach[3] on rocks. In the studies on ceramics, tests have been performed on both unconfined (bare) and laterally confined (sleeved with a ductile alloy) bars. Brar et al.[4] performed the first series of impact tests on unconfined 12.7-mm diameter Coors 94% and 99.8% alumina bars to determine the amplitude of the propagating stress wave (in-situ stress) as a function of the impact stress generated by a steel flyer plate launched at 100-500 m/s. They reported that a constant amplitude stress (~ static strength of the material) wave was produced when the impact stress was below or equal to the compressive yield stress of alumina. In the tests, where the impact stress exceeded the yield stress, loading stress in the bar decayed with distance and time due to lateral release involving dilatancy. In the second series of bar impact experiments, Brar and Bless[5] employed a high-speed photographic technique, in conjunction with in-situ measurements of axial stress induced by plate and bar impactors, to observe the fracture and failure modes of a number of ceramics (Al_2O_3, B_4C, SiC, TiB_2) and glass (pyrex). They concluded that failure in B_4C, SiC, TiB_2, and pyrex bar takes place by a propagating destruction wave, whereas alumina fails through axial splitting leading to faulting.

Cosculluela et al.[6] impacted 10-mm diameter T299 alumina (density=3.86 g/cm^3) bars with tungsten alloy impactor plates at velocities ranging form 80 to 700 m/s. Material velocity histories were measured at 8, 10, and 12-cm from the impact face of the bars. Lagrangian analysis of the velocity histories showed that highest stress amplitude wave that

propagates in the alumina bar is 3.2 GPa, regardless of the impactor velocity. Microscopic examination of the softly recovered impacted specimens suggested that cracks nucleate and grow until uni-axial stress in the bar approaches the maximum strength of the specimen.

Wise and Grady[7] performed impact tests on unconfined and confined (in close-fitting tantalum sleeve) Coors 99.5% alumina bars with aluminum flyer plates launched at velocities from 1035 to 2182 m/s. They measured a maximum in-situ axial stress in unconfined bars of 3.15 GPa, irrespective of the impactor velocity, as observed by Cosculluela et al.[6] on similar alumina bars. Furthermore, the maximum in-situ stress value of 3.15 GPa was lower than the dynamic yield strength of 4.3 GPa of the material, suggesting a pressure dependence of the yield strength of alumina. Maximum in-situ axial stress in confined alumina bars is about twice (6.1 GPa) the value for the unconfined bars. This increase in measured axial stress was interpreted by the authors in terms of confinement, consistent with expected upper dynamic limit equal to the HEL of alumina (6.2 GPa). Simha[8] also reported a similar increase in measured in-situ axial stress (4.2 GPa) in 12.7-mm diameter confined (with a steel sleeve) Coors 99.5% alumina bars (6 diameters long) compared to that (3.7 GPa) in unconfined bars.

Chhabildas et al.[9] extended Wise and Grady's study to determine differences, if any, in measured in-situ axial stress in bare (unconfined) and sleeved (in shrink fit steel cylinder) 99.5% alumina bars impacted by a graded density flyer plate versus a single density (steel) impactor plate launched at 300-366 m/s. The authors explain the slight increase in maximum loading stress with a graded density flyer plate on the basis of delayed lateral release, due to a longer rise time for the loading stress wave. The measured in-situ axial stress in unconfined bars was slightly higher (3.5 GPa), when impacted with a graded density flyer plate compared to that (3.4 GPa) with a single density (steel) impactor. In sleeved bar targets, measured in-situ axial stress was in the range of 4.6 to 5.1 GPa, significantly higher than in the case of unconfined bars, in agreement with earlier studies. Tensile waves generated as a result of lateral release in a sleeved bar target are totally eliminated during the initial loading stress wave.

1.2 Numerical Simulation of Bar Impact Experiments

Cosculluela et al.[6] simulated free surface velocity histories at 8, 10, and 12 diameters away from the impact face of alumina (T299) bars impacted with steel plate impactors, using ABAQUS and EPIC3 computer codes. Simulations showed that state of stress in the bar transforms from uni-axial strain to uni-axial stress at a distance equal to two times the bar diameter. Simulated peak axial stress, 3.9 GPa, was greater than the measured value of 3.2 GPa. Physical evidence of the effect of the change from uni-axial strain to uni-axial stress is provided by the length of damaged portion observed in high-speed photographs of alumina bars impacted by similar bars (Brar and Bless[4]). The damage as a result of axial splitting due to failure in tension is confined to two diameters from the impact face. Espinosa and Brar[10] simulated the alumina bar impacts[4,8] using the multi-plane microcracking model. The simulations (Figure 1) capture qualitatively the long and stable pulse duration observed at the lowest impact velocity (99 m/s) because the material remains undamaged. When the impact stress exceeds a material threshold (static compressive strength), simulations do not match the detailed features observed in measured axial stress-time profiles. Simulated peak axial stress and detailed features in axial stress histories are very sensitive to the assumed values of radii (1 μm, 10 μm, and 20 μm) of microcracks in alumina bars (Figure 1). Furthermore, the oscillations in simulated axial stress histories are attributed to the spatial resolution of the mesh size used in simulations. Simulations predict only the trend in the duration of the stress wave in the bar becoming shorter as the impact stress is increased above the material threshold. Pulse duration is controlled by the rate of unconfined compressive damage, the quantification of which is based on the complex material model parameters.

Simha[8] has developed a damage based constitutive model for 99.5% alumina to simulate the 99.5% alumina bar-on-bar impact stress histories. The model parameters for 99.5% alumina are based on constitutive relationships inferred from plate impact and bar impact data on 99.5% alumina (Grady and Moody[11], Dandekar and Bartowski[12], and Bourne et al.[13]). Damage accumulation is modeled as a scalar isotropic damage variable used to soften the shear modulus and computational cells fail in tension when a critical level of damage is reached. Simulated axial stress profiles of Simha's bar-on-bar impact

tests do not match any features in the measured axial stress histories [14]. Using his constitutive model for 99.5% alumina, Simha[15] also attempted to simulate velocity histories in bar impact experiments on unconfined and confined (sleeved) 99.5% alumina bars by Chabbildas et al.[9]. These simulations matched the measured peak velocity only, missing all the detailed features, including the timings in initial rise of the profile (Figure 2). Grove and Rajendran[16] followed a similar approach to develop R-G model for 99.5% alumina from flyer plate data. They used the R-G model parameters for 99.5% alumina to simulate the free-surface velocity profiles in bar impact experiments due to Chhabildas et al[9]. The simulated velocity histories in bar impact test configurations agreed with the measurements only in the shots when the alumina bar target had a steel sleeve around it. In the case of unconfined bar targets simulated velocity histories were significantly lower than the measured data (Figure 3).

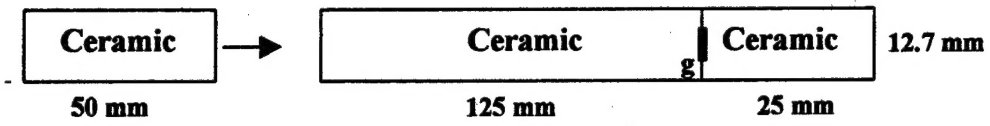

(a)

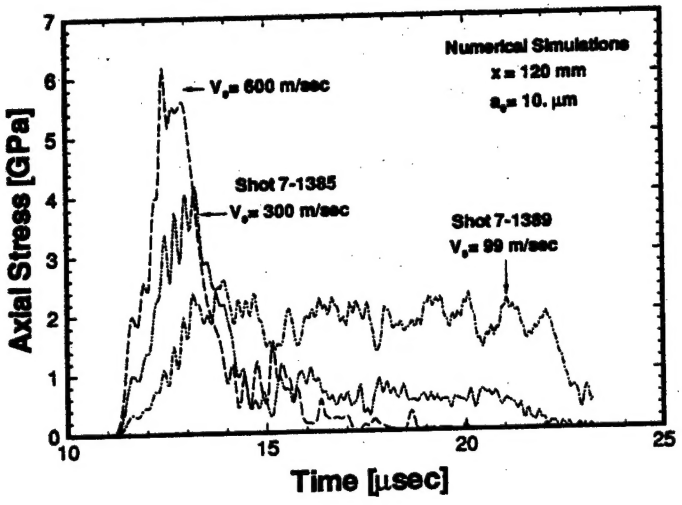

(b)

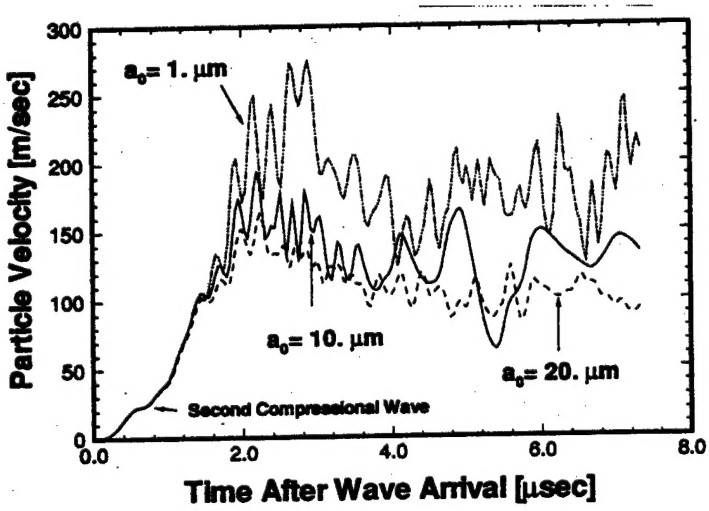

(c)

Figure 1. (a) Schematic of ceramic bar-on-bar experiment, (b) Computed axial stress histories for 99, 300, and 600 m/s impact velocities in alumina bars, and (c) Axial velocity histories at the target bar free end for three different initial microcrack radii (Reference 10).

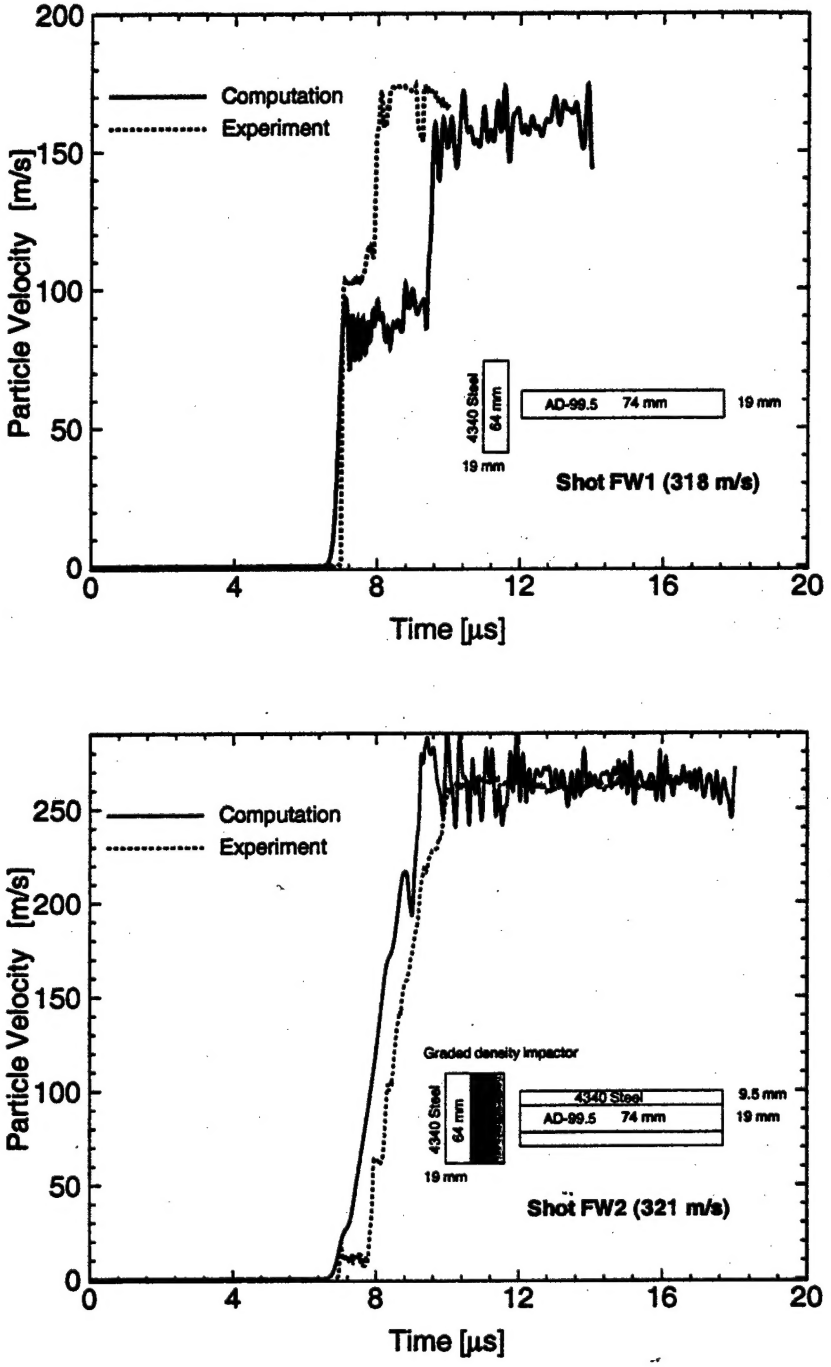

Figure 2. Comparison of simulated (Simha's model) and measured velocity histories in unconfined and sleeved AD-99.5 bar impact experiments reported in Reference 9.

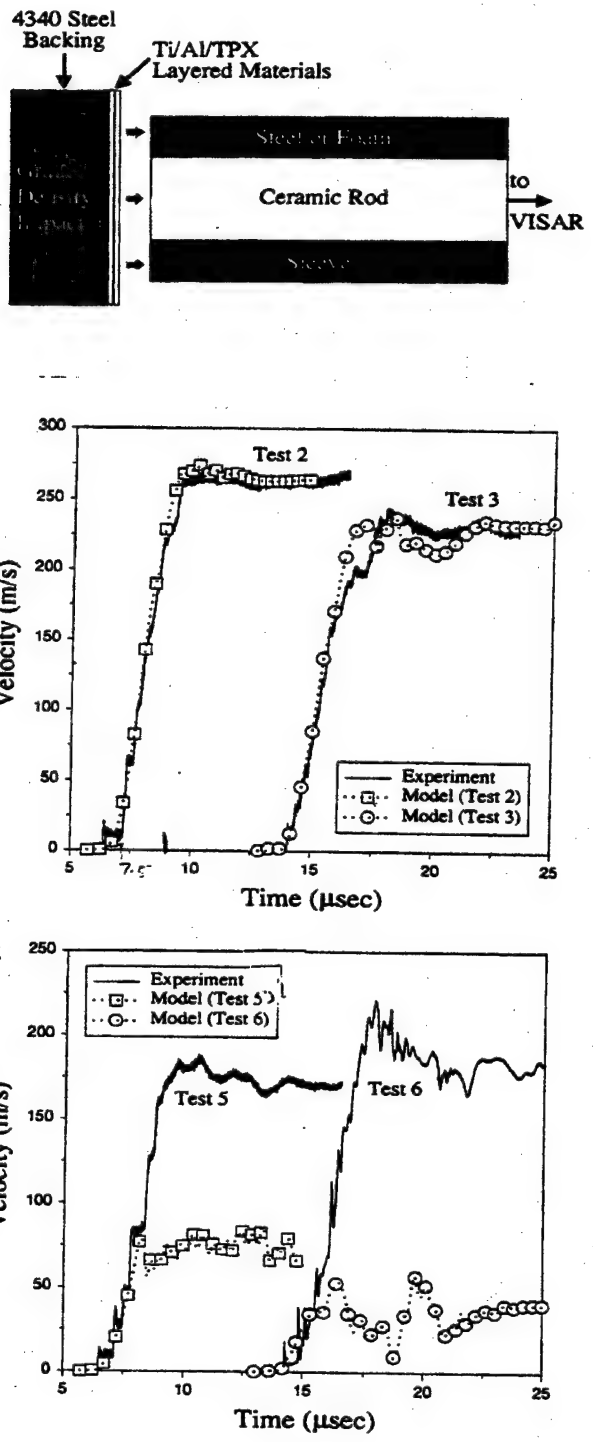

Figure 3. (a) Schematic of the experimental configuration of a graded density flyer plate impacting a AD-99.5 bar target. Comparison of simulated (RG model) and measured velocity profiles for (b) sleeved AD-99.5 bars and (c) unconfined AD-99.5 bars, (Reference 16).

SECTION 2
CERAMIC BAR-ON-BAR IMPACT EXPERIMENTS AND RESULTS

A total of six bar-on-bar impact experiments were performed at the 50-mm gas gun facility of the University of Cambridge on 12.7-mm diameter Coors AD-998 alumina bars at nominal impact speeds of 100 m/s, 200m/s, and 300m/s. A schematic of the ceramic bar-on-bar experiment is shown in Figure 4. The shot matrix is summarized in Table 1. The free surface velocity of the far end of the target bar was measured using a VISAR. Fracture and failure modes of impactor and target bars are photographed using a high-speed (Imacon) camera operating at 10^5 frames/s. The images are provided in Appendix A. The measured free surface velocity data and high-speed photographs are to be shared with various researchers engaged in developing constitutive models for armor ceramics.

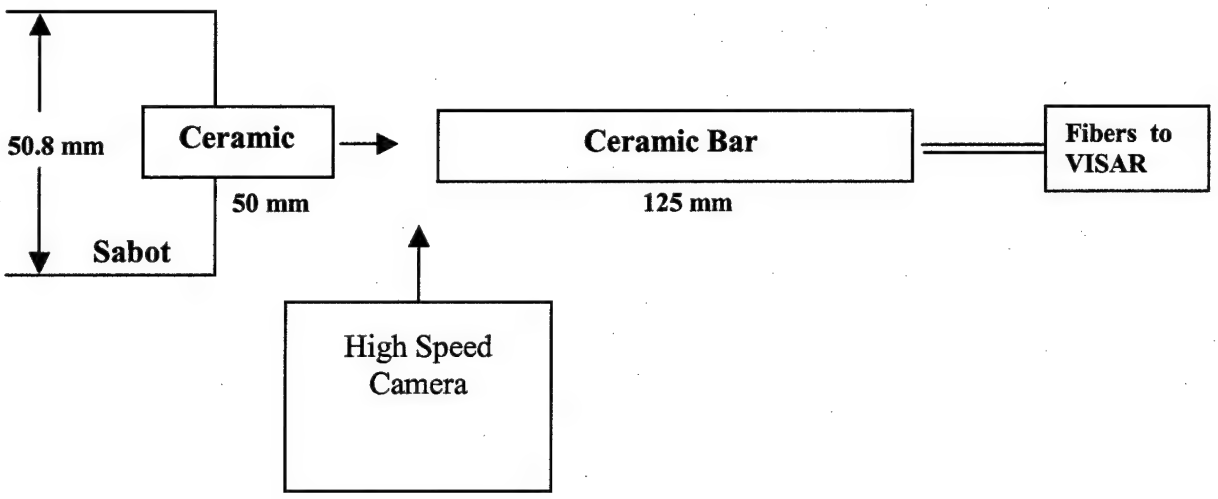

Figure 4. Schematic of the ceramic bar-on-bar impact experiment.

Measured free surface velocity-time data for the six shots are shown in Figures 5-7 in three pairs: (i) shots 021106a and 0211106b at impact velocities of 112.2 m/s and 112.5 m/s, (ii) shots 021025b and 021028c at impact velocities of 220.8 m/s and 222.8 m/s, and (iii) shots 021022a and 021025a at impact velocities of 295.7 m/s and 298.6 m/s. Free surface velocities for the two shots at 112.2 m/s and 112.5 m/s agree within about 7%. Similar agreement between the free surface velocities for the two shots at ~220 m/s and two at ~ 300 m/s was observed.

Table 1. Summary of AD998 Alumina Bar-on-Bar Impact Shots

Shot No	Shot ID	Projectile Mass (g)	Velocity ($m\ s^{-1}$)	Interframe time (μs)	Remarks
1	021022a	275	295.7	5	VISAR and High Speed Camera
2	021025a	275	298.6	5	VISAR and High Speed Camera
3	021025b	1006	220.8	5	VISAR and High Speed Camera
4	021028c	1006	222.3	20	VISAR and High Speed Camera
5	021106a	1006	112.2	20	VISAR and High Speed Camera
6	021106b	1006	112.5	20	VISAR and High Speed Camera

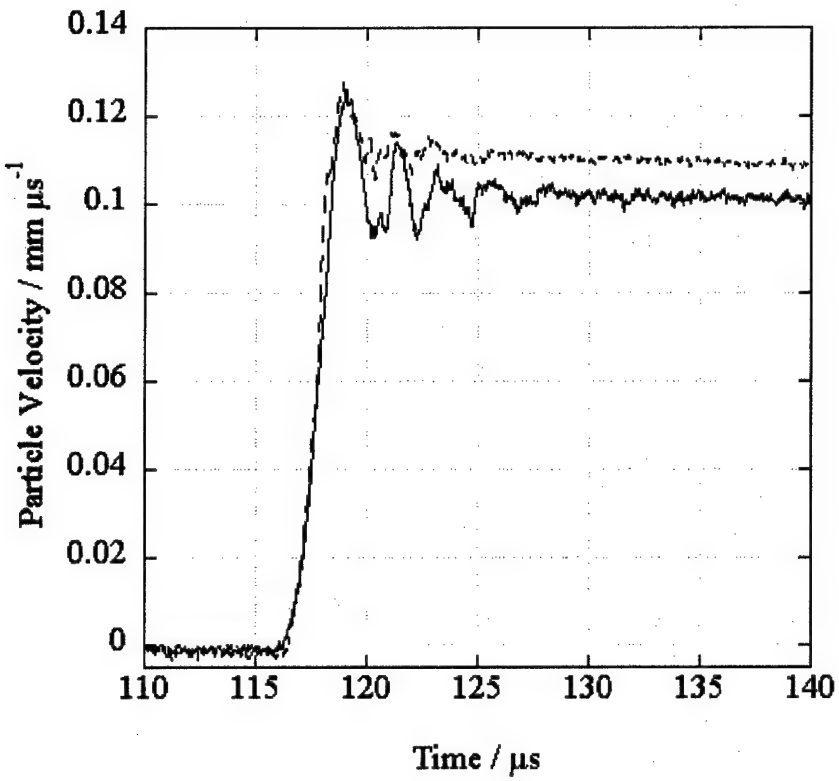

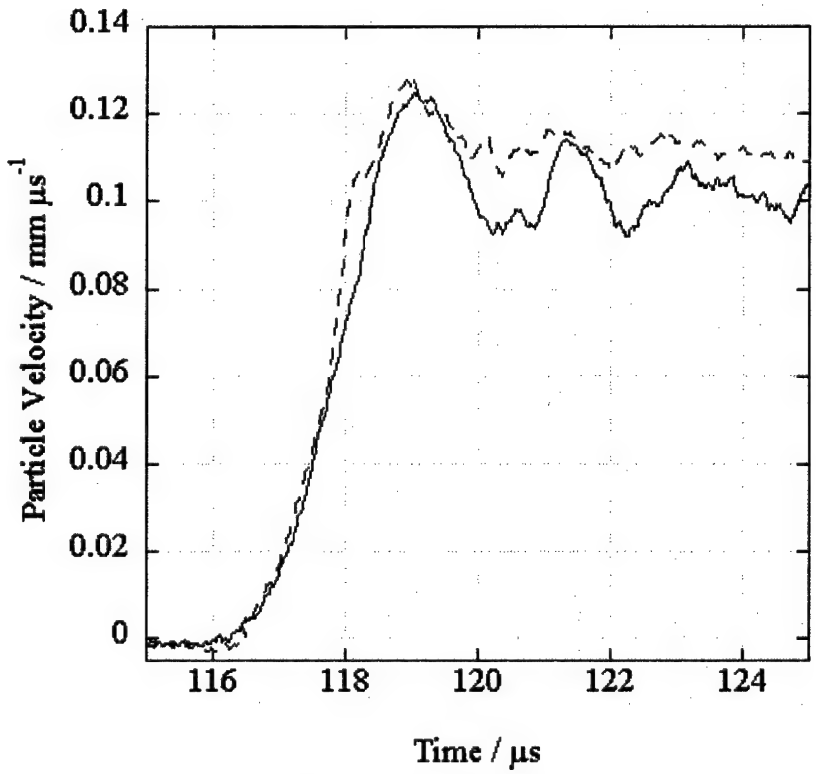

Figure 5. Free surface velocity in alumina bar-on-bar impact at 112 m/s; top view data from entire impact event and bottom view for the first 5 μs.

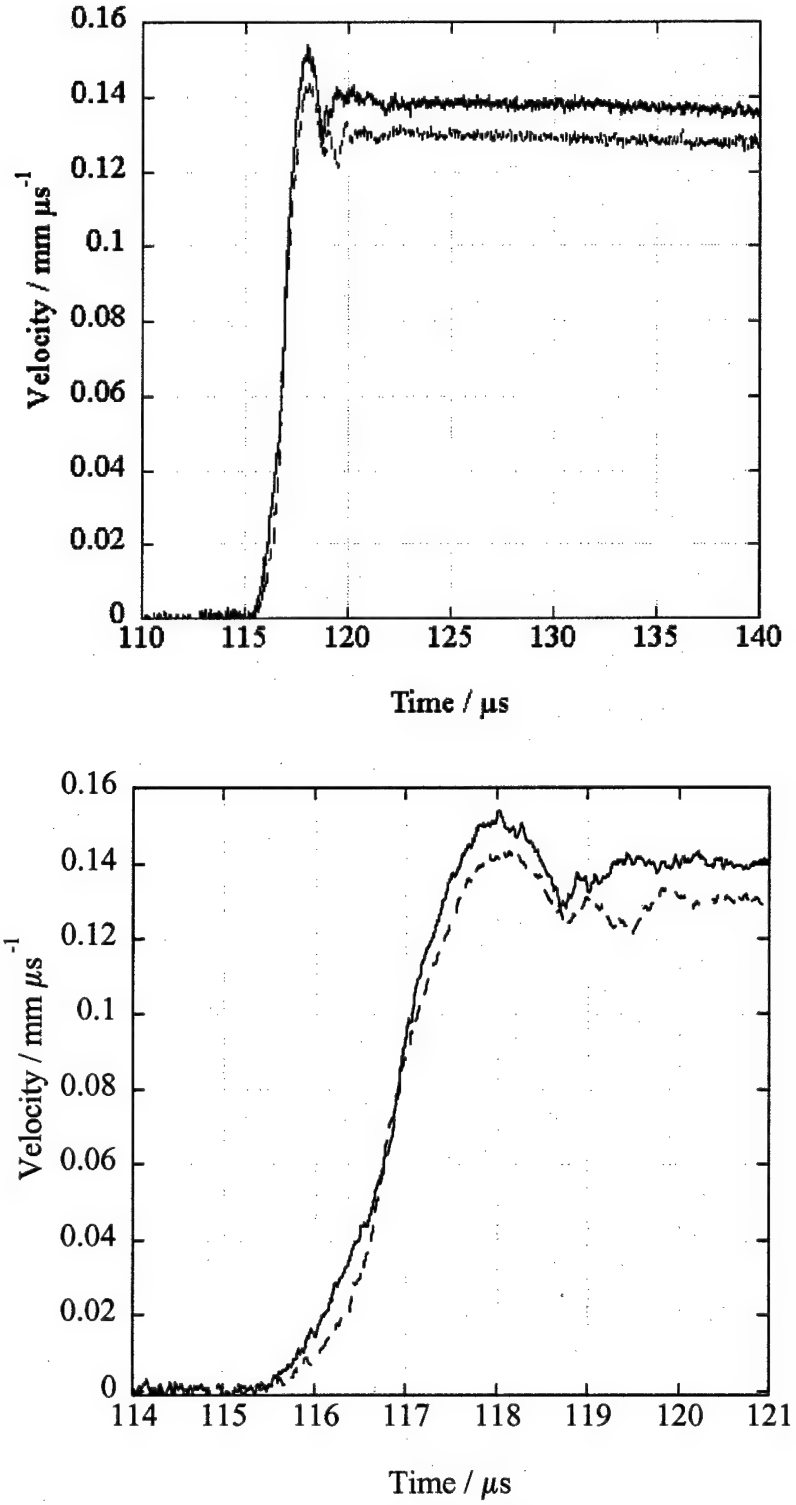

Figure 6. Free surface velocity in alumina bar-on-bar impact at 222.3 m/s and 220.8 m/s; top view data from entire impact event and bottom view for the first 5 μs.

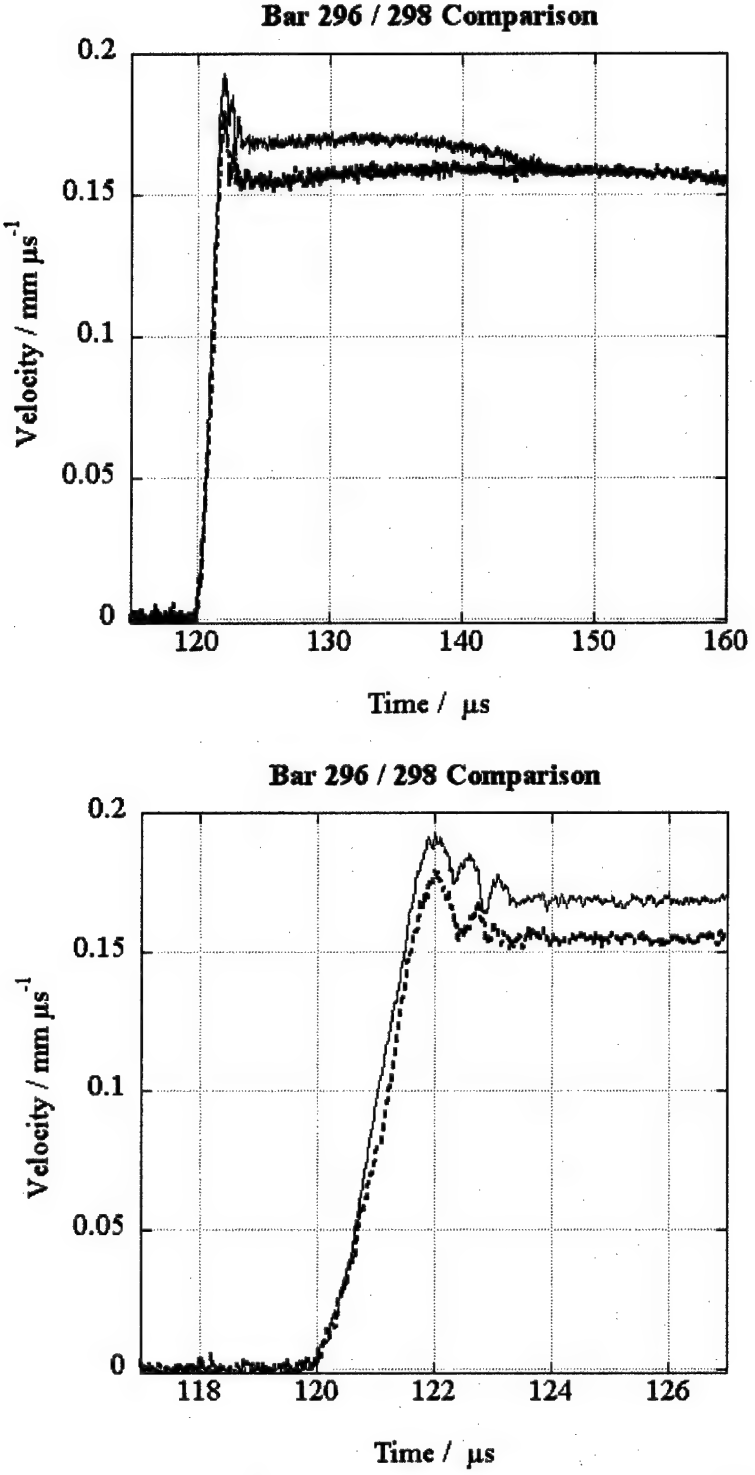

Figure 7. **Free surface velocity for alumina bar-on-bar impact at 295.6 m/s and 298 m/s; top view for the entire impact event and bottom for the first 7 μs.**

SECTION 3
CONCLUSIONS

Velocity history data from ceramic bar-on-bar impact experiments obtained using a VISAR presented in this report. These data are the first of its kind. In most of the earlier ceramic bar-on-bar impact experiments axial stress was measured with embedded manganin stress gauges. These stress-time data depended on the survival of the manganin gauges and in many instances the gauge failed prematurely resulting in incomplete data from the impact event. In cases where VISAR was employed to record velocity history of the far end of the target bar, the impact stress was introduced using a flyer plate rather than a bar to suppress axial splitting during the impact event.

Measured velocity history data (particle velocity vs time) from the two shots at the lowest impact velocity of 112 m/s (Figure 5) agree within 7%. Average peak particle velocities of 105 m/s and 112 m/s from the two shots exhibit an elastic response of AD-998 alumina bars at this impact velocity. Measured particle velocities in the other four shots, two at ~220 m/s and the other two at ~295 m/s show a variation of ~10% between each pair of shots. These data further show that alumina bar impact response at these higher impact velocities is inelastic. These observations are in agreement with earlier studies on the failure of impacted alumina bars through axial splitting.

We propose future the alumina bar-on-bar impact experiments be performed by confining the target and impact bar in metal sleeves providing varying levels of confinement stress around the bars. The confinement stress would delay and inhibit the premature failure of the bars through axial splitting. Velocity history data from these experiments will provide ceramic bar impact data under one more impact geometry to the researchers engaged in generating material models for armor ceramics.

SECTION 4
REFERENCES

1. Z. Rosenberg, M. Mayseless, and Y. Partom, The use of manganin stress transducers in impulsively loaded long rod experiments, Trans. ASME, **51**, pp. 202-4, 1984.
2. Z. Rosenberg and S. J. Bless, Determination of dynamic yield strengths with embedded manganin gauges in plate-impact and long-rod experiments, Exp. Mech., **26**, pp. 279-82, 1986.
3. W. Janach, Int. J. Rock Mech. Min. Sci., Geomech. Abstr., **13**, pp. 177-80, 1976.
4. N. S. Brar, S. J. Bless, and Z. Rosenberg, Brittle failure of ceramic rods under dynamic compression, DYMAT 88, J. de Physique, **49**, Suppl. 9, pp. C-3-607-12, 1988.
5. N. S. Brar and S. J. Bless, Dynamic fracture and failure mechanisms of ceramic bars, Shock-Wave and High-Strain-Rate Phenomena in Materials, Eds. M. A. Meyers et al., Marcel Dekker, Inc, pp. 1041-49, 1992.
6. A. Cosculluela, J. Cagnoux, and F. Collombet, Two types of experiments for studying uniaxial dynamic compression of alumina, Shock Compression of Condensed Matter-1991, Eds. S. C. Schmidt et al., Elsevier Science Publishers, pp. 951-54, 1992.
7. J. L. wise and D. E. Grady, Dynamic multiaxial impact response of ceramic rods, High Pressure Science and Technology-1993, Eds. S. C. Schmidt et al., AIP Conference Proceedings 309, New York, pp. 777-80, 1992.
8. C. M. Simha, High Rate Loading of a High Purity ceramic-1-D Stress Experiments and Constitutive Modeling, Ph. D. Thesis, University of Texas, Austin, 1998.
9. L. C. Chhabildas, M. D. Furnish, W. D. Reinhart, and D. E. Grady, Impact of AD995 Alumina Rods, Shock Compression of Condensed Matter-1997, Eds. S. C. Schmidt et al., AIP Conference Proceedings 429, New York, pp. 505-08, 1998.
10. H. D. Espinosa and N. S. Brar, Dynamic Failure Mechanisms of Ceramic Bars: Experiments and Numerical Simulations, J. Mech. Phys. Solids, **43**, pp. 1615-38, 1995.
11. D. E. Grady and R. L. Moody, Shock compression profiles in ceramics, Sandia Technical report SAND96-0551, Sandia National Laboratories, 1996.
12. D. P. Dandekar and P. Bartkowski, Shock response of AD-995 alumina, High Pressure Science and Technology-1993, Eds. S. C. Schmidt et al., AIP Conference Proceedings 309, New York, pp. 777-80, 1992.
13. N. Bourne, J. Millet, Z. Rosenberg, and N. Murray, On the shock induced failure of brittle solids, J. Mech. Phys. Solids, **46**, pp. 1887-1908, 1998.
14. C. M. Simha, S. J. Bless, and A. Bedford, What is the peak stress in ceramic bar impact experiments?, Shock Compression of Condensed Matter-1999, Eds. M. D. Furnish et al., AIP Conference Proceedings 505, pp. 615-18, 2000.

15. C. M. Simha, S. J. Bless, and A. Bedford, Computational modeling of the penetration response of a high-purity ceramic, Int. J. of Impact Engineering, **27**, pp. 65-86, 2002.

16. D. J. Grove and A. M. Rajendran, Modeling of microcrack density based damage evolution in ceramic rods, Shock Compression of Condensed Matter-1999, Eds. M. D. Furnish et al., AIP Conference Proceedings 505, pp. 619-22, 2000.

APPENDIX A

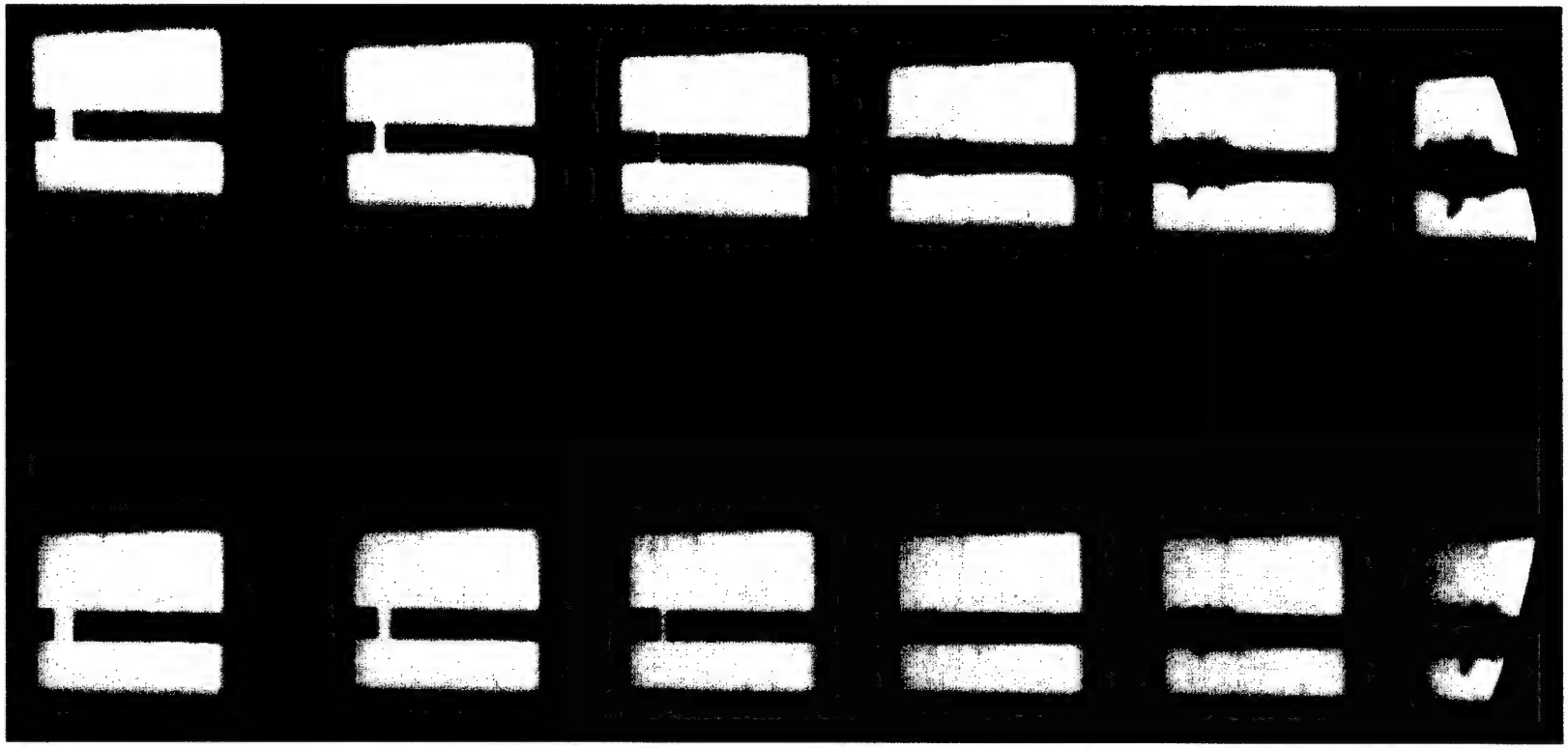

Figure A1. **Sequence of high-speed (Imacon) photographs of shot 021022a (295.7 m/s) showing the impactor bar moving from left striking the target bar on the right. First and second frames are on the left in the lower and the upper series of frames, respectively, and the interframe time is 5 μs.**

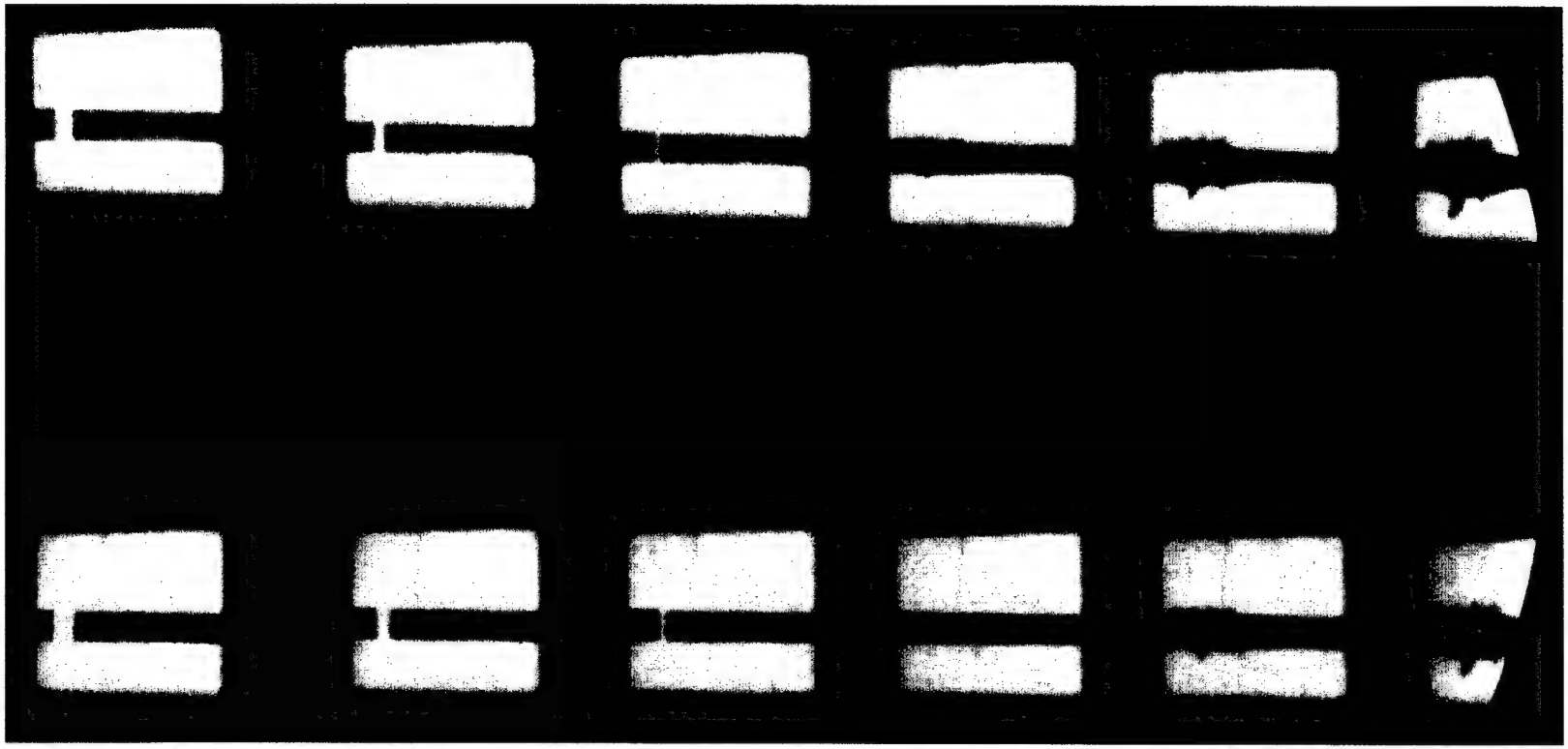

Figure A2. **Sequence of high speed (Imacon) photographs of shot 021025a (298.6 m/s) showing the impactor bar moving fromleft striking the target bar on the right. First and second frames are on the left in the lower and the upper series of frames, respectively, and the interframe time is 5 μs.**

Figure A3. **Sequence of high-speed (Imacon) photographs of shot 021025b (220.8 m/s) showing the impactor bar moving from left striking the target bar on the right. First and second frames are on the left in the lower and the upper series of frames, respectively, and the interframe time is 5 μs.**

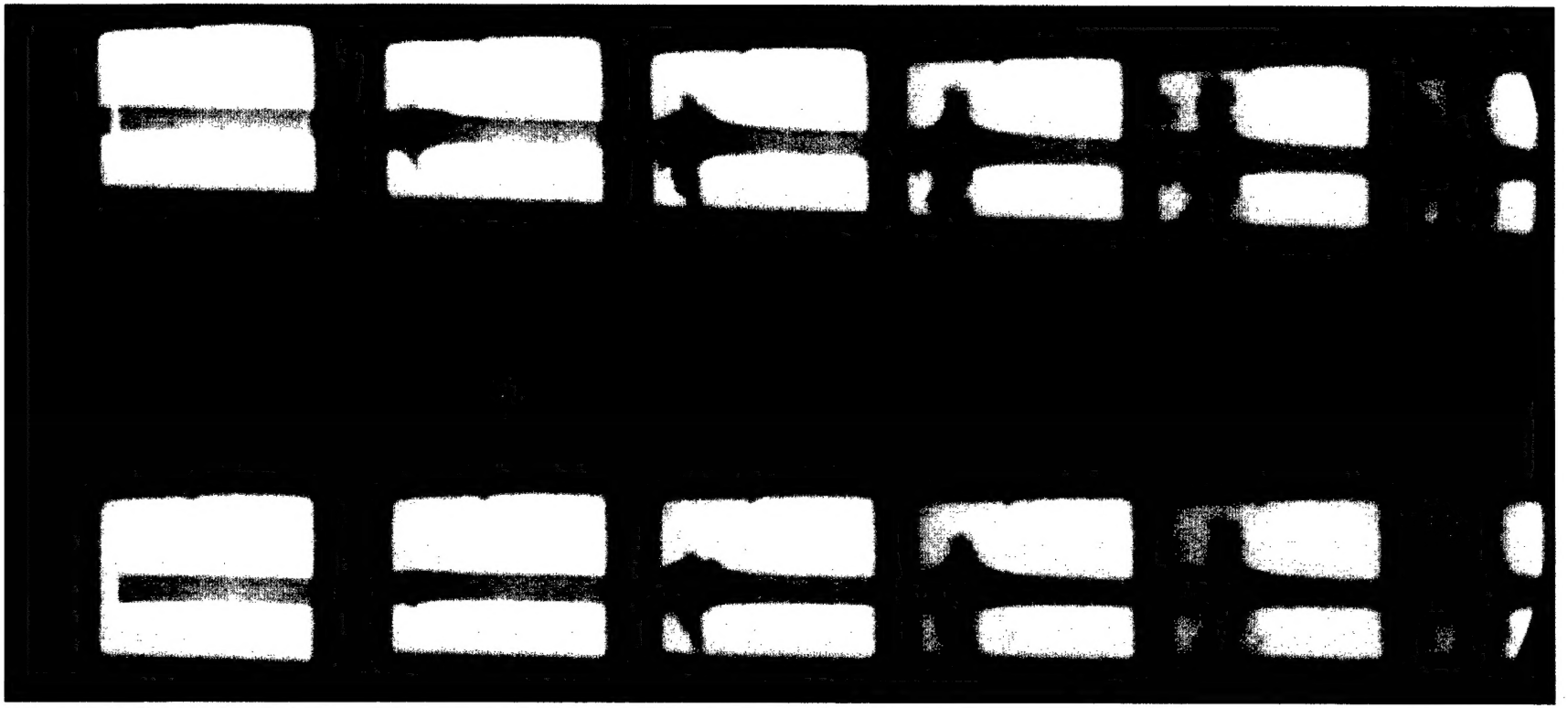

Figure A4. **Sequence of high-speed (Imacon) photographs of shot 021028c (222.3 m/s) showing the impactor bar moving from left striking the target bar on the right. First and second frames are on the left in the lower and the upper series of frames, respectively, and the interframe time is 20 μs.**

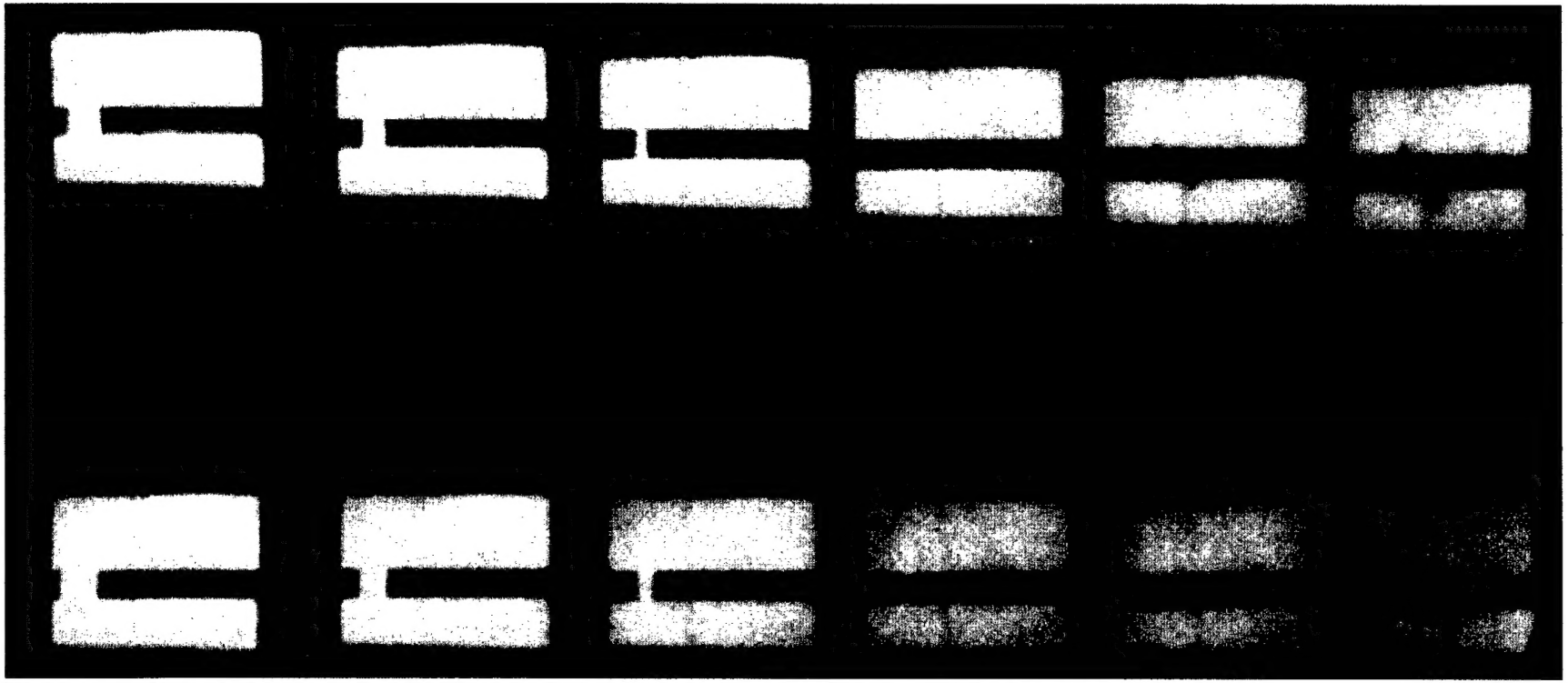

Figure A5. **Sequence of high-speed (Imacon) photographs of shot 021106a (112.2 m/s) showing the impactor bar moving from left striking the target bar on the right. First and second frames are on the left in the lower and the upper series of frames, respectively, and the interframe time is 20 μs.**

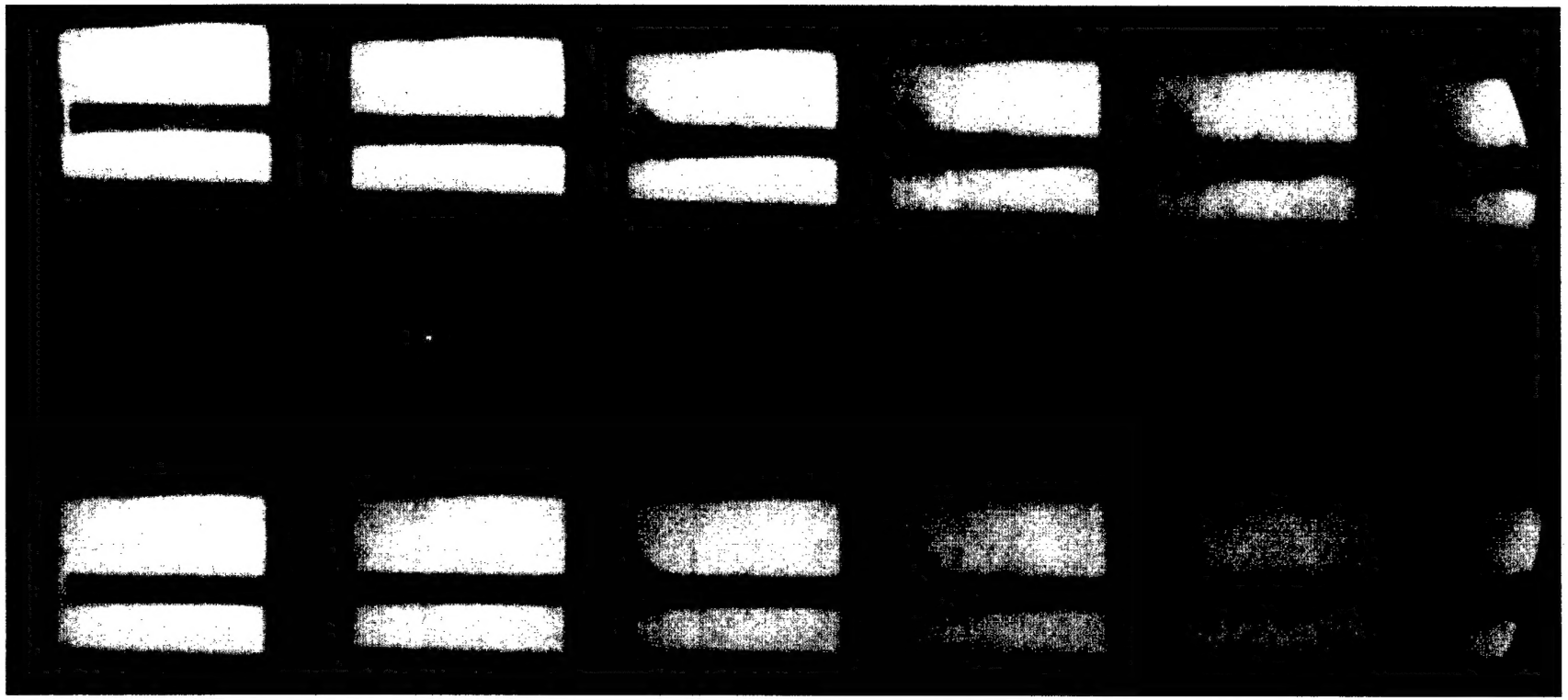

Figure A6. **Sequence of high-speed (Imacon) photographs of shot 021106b (112.5 m/s) showing the impactor bar moving from left striking the target bar on the right. First and second frames are on the left in the lower and the upper series of frames, respectively, and the interframe time is 20 μs.**